



<b>Publication Year</b>	2022
<b>Acceptance in OA</b>	2022-03-18T15:55:43Z
<b>Title</b>	An Algorithm to Calibrate and Correct the Response to Unpolarized Radiation of the X-Ray Polarimeter Onboard IXPE
<b>Authors</b>	RANKIN, JOHN, MULERI, FABIO, Tennant, Allyn F., BACHETTI, Matteo, COSTA, ENRICO, DI MARCO, Alessandro, FABIANI, Sergio, LA MONACA, FABIO, SOFFITTA, PAOLO, TOBIA, ANTONINO, TROIS, ALESSIO, XIE, FEI, Baldini, Luca, Di Lalla, Niccolo, Manfreda, Alberto, O'Dell, Stephen L., PERRI, Matteo, Puccetti, Simonetta, Ramsey, Brian D., Sgro, Carmelo, Weisskopf, Martin C.
<b>Publisher's version (DOI)</b>	10.3847/1538-3881/ac397f
<b>Handle</b>	<a href="http://hdl.handle.net/20.500.12386/31726">http://hdl.handle.net/20.500.12386/31726</a>
<b>Journal</b>	THE ASTRONOMICAL JOURNAL
<b>Volume</b>	163



# An Algorithm to Calibrate and Correct the Response to Unpolarized Radiation of the X-Ray Polarimeter Onboard IXPE

John Rankin<sup>1,2,3</sup> , Fabio Muleri<sup>1</sup> , Allyn F. Tennant<sup>4</sup>, Matteo Bachetti<sup>5</sup> , Enrico Costa<sup>1</sup> , Alessandro Di Marco<sup>1</sup> , Sergio Fabiani<sup>1</sup> , Fabio La Monaca<sup>1</sup> , Paolo Soffitta<sup>1</sup> , Antonino Tobia<sup>1</sup>, Alessio Trois<sup>5</sup>, Fei Xie<sup>1</sup>, Luca Baldini<sup>6,7</sup> , Niccolò Di Lalla<sup>8</sup> , Alberto Manfreda<sup>7</sup> , Stephen L. O'Dell<sup>4</sup>, Matteo Perri<sup>9</sup> , Simonetta Puccetti<sup>10</sup> , Brian D. Ramsey<sup>4</sup>, Carmelo Sgrò<sup>7</sup> , and Martin C. Weisskopf<sup>4</sup>

<sup>1</sup> Istituto di Astrofisica e Planetologia Spaziali di Roma, Via Fosso del Cavaliere 100, I-00133 Roma, Italy; [john.rankin@inaf.it](mailto:john.rankin@inaf.it)

<sup>2</sup> Università di Roma Sapienza, Dipartimento di Fisica, Piazzale Aldo Moro 2, I-00185 Roma, Italy

<sup>3</sup> Università di Roma Tor Vergata, Dipartimento di Fisica, Via della Ricerca Scientifica, 1, I-00133 Roma, Italy

<sup>4</sup> NASA Marshall Space Flight Center, Huntsville, AL 35812, USA

<sup>5</sup> INAF/Osservatorio Astronomico di Cagliari, Via della Scienza 5, I-09047 Selargius (CA), Italy

<sup>6</sup> Università di Pisa, Dipartimento di Fisica Enrico Fermi, Largo B. Pontecorvo 3, I-56127 Pisa, Italy

<sup>7</sup> Istituto Nazionale di Fisica Nucleare, Sezione di Pisa, Largo B. Pontecorvo 3, I-56127 Pisa, Italy

<sup>8</sup> W.W. Hansen Experimental Physics Laboratory, Kavli Institute for Particle Astrophysics and Cosmology, Department of Physics and SLAC National Accelerator Laboratory, Stanford University, Stanford, CA 94305, USA

<sup>9</sup> INAF/Osservatorio Astronomico di Roma, Via Frascati 33, I-00040, Monte Porzio Catone (RM), Italy

<sup>10</sup> Agenzia Spaziale Italiana, Via del Politecnico snc, I-00133 Roma, Italy

Received 2021 September 14; revised 2021 November 11; accepted 2021 November 12; published 2022 January 4

## Abstract

The Gas Pixel Detector (GPD) is an X-ray polarimeter to fly onboard IXPE and other missions. To correctly measure the source polarization, the response of IXPE's GPDs to unpolarized radiation has to be calibrated and corrected. In this paper, we describe the way such response is measured with laboratory sources and the algorithm to apply such correction to the observations of celestial sources. The latter allows to correct the response to polarization of single photons, therefore allowing great flexibility in all the subsequent analysis. Our correction approach is tested against both monochromatic and nonmonochromatic laboratory sources and with simulations, finding that it correctly retrieves the polarization up to the statistical limits of the planned IXPE observations.

*Key words:* Polarimeters – X-ray telescopes – X-ray observatories – X-ray detectors

## 1. Introduction

Astronomical X-ray polarimetry has up until now seen significative detections only of the Crab Nebula (Weisskopf et al. 1978; Feng et al. 2020), but this unexplored window will soon be reopened thanks to the IXPE mission (Weisskopf et al. 2016; Soffitta et al. 2021), with the onboard polarization-sensitive Gas Pixel Detector (GPD; Costa et al. 2001; Bellazzini et al. 2006, 2007). This device has already flown onboard the PolarLight cubesat mission (Feng et al. 2019), providing new results on the Crab Nebula, and it will also fly on future missions (e.g., eXTP (Zhang et al. 2019)).

Expected polarization from X-ray astronomical sources is higher than at longer wavelengths, e.g., optical or infrared, but still a few percent of the source signal. At this level, IXPE's GPDs—and often other real X-ray polarimeters—show systematic effects that mimic the signal generated by a genuine source polarization even for truly unpolarized radiation (Baldini et al. 2021). Due to the characteristics of this effect, and to facilitate its correction, part of it will be compensated by the fact that IXPE's observations will be dithered (i.e., the pointing direction of the telescope will oscillate during the observations, distributing source photons over a relatively large region, nearly uniformly illuminated and centered on the field of view). The remainder of these systematic effects need to be calibrated (F. Muleri et al. 2021, in preparation) and removed

before being able to achieve the statistical limit of the polarization measurement.

In this paper, we describe the algorithm to calibrate and correct the response of IXPE's GPDs to unpolarized radiation in order to remove the spurious instrumental signal, referred to as spurious modulation. First, we describe how the response of the detector to unpolarized radiation is measured. This method gives, as a byproduct, the corrected polarization of the laboratory sources.

We then present the algorithm that will be used for the correction of celestial observations. It is able to remove the systematic effect from individual photon events, therefore rendering the subsequent analysis flexible. This method comprises two parts: the creation of a calibration database containing spatial and spectral information on the systematic effect, and the subtraction of the systematic effect from each single photon detected by using the spatial information and interpolating the spectral information.

We compare, for monochromatic sources, the polarization obtained by using this correction algorithm with that obtained as a byproduct of the unpolarized response measurement. We also study the application of the correction method to nonmonochromatic sources. The algorithm is further tested using toy simulations to verify that statistical uncertainties are propagated correctly.

This paper is structured as follows. In Section 2, we describe how the GPD measures X-ray polarization. The method used to measure the response to unpolarized radiation is presented in Section 3, while the photon-by-photon correction algorithm is described in Section 4. The testing of this algorithm applied to



Original content from this work may be used under the terms of the [Creative Commons Attribution 4.0 licence](https://creativecommons.org/licenses/by/4.0/). Any further distribution of this work must maintain attribution to the author(s) and the title of the work, journal citation and DOI.

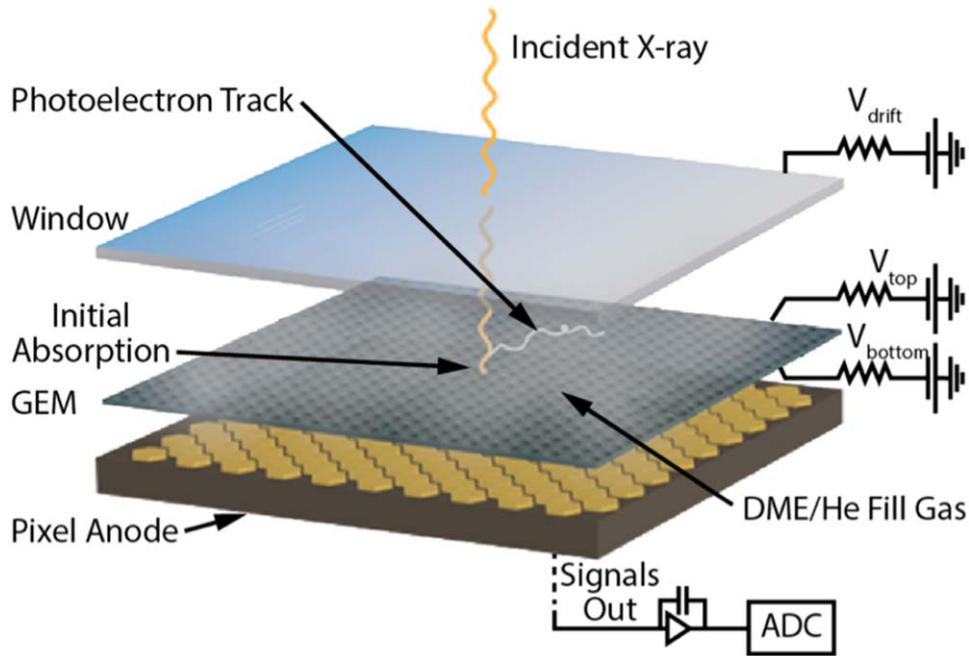


Figure 1. Schematic of the GPD. See the text for details. Image credit: Weisskopf et al. (2016)

laboratory X-ray sources and to simulations is reported in Section 5. Finally, in Section 6, conclusions are drawn.

## 2. The Gas Pixel Detector

The Gas Pixel Detector (GPD) is a polarization-sensitive X-ray detector able to perform spatially, timing, and spectrally resolved polarization measurements. This detector (Baldini et al. 2021) is the core of the IXPE instrument (Soffitta et al. 2021), and is scheduled to fly onboard the IXPE mission. The measurements in this article were acquired at INAF-IAPS during the ground calibration of the Detector Units (F. Muleri et al. 2021, in preparation; Fabiani et al. 2021), with INAF-IAPS’s calibration equipment (Muleri et al. 2022). The IXPE instrument consists of three detector units (each containing a GPD) with three corresponding X-ray optics. The data used in this paper were taken from detector unit number 2, and are representative of the results obtained with the other detector units.

A schematic view of the GPD is shown in Figure 1. The functioning is the following. An incident X-ray enters through the beryllium window and is absorbed in the gas cell filled with DME. The absorption of the photon causes the production of a photoelectron, which propagates in the gas, producing an ionization track. Such a charge is collected with a drift field, multiplied by a gas electron multiplier, and eventually is collected by a custom ASIC specifically developed for these detectors.

### 2.1. Polarization Measurement

The direction of emission of photoelectrons is statistically more probable parallel to the position angle of the polarization. Therefore, the response of the instrument is essentially the distribution of the (azimuthal) directions of the photoelectrons, referred to as the modulation curve. In cases where the incident radiation is unpolarized, the distribution is expected to be flat, except for statistical fluctuations due to the finite number of acquired photons (Figure 2, upper right). In cases where the incident radiation is polarized, the distribution of photoelectrons is expected to be modulated as a  $\cos^2$  (Figure 2, left).

The “classical” approach to derive the polarization degree and angle is to fit the distribution as  $N(\phi) = A + B \cos^2(\phi - \varphi_0)$  and derive the so-called modulation from the parameters of the fit as  $m = \frac{\max(N) - \min(N)}{\max(N) + \min(N)} = \frac{B}{2A + B}$ . The polarization degree is then given by

$$p = \frac{m}{\mu(E)}, \quad (1)$$

where  $\mu$  is the modulation factor, equal to the modulation when the incident radiation is 100% polarized and dependent on the energy  $E$ . The polarization position angle  $\varphi_0$  coincides with the peak of the modulation curve.

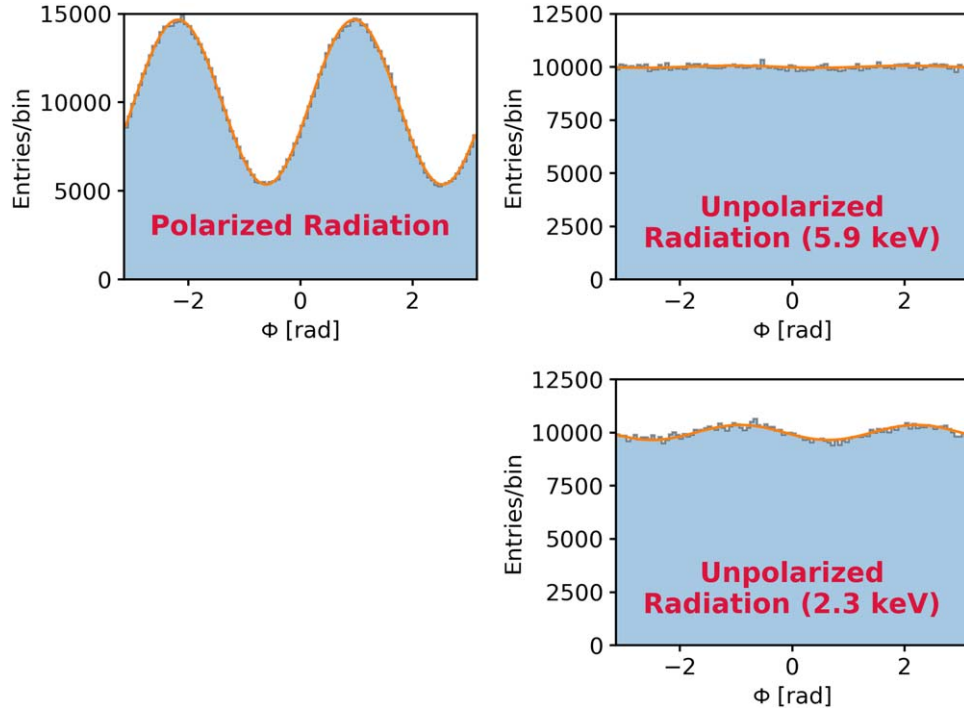
However, this approach has two shortcomings with respect to the goal of this paper. First, because the polarization degree and phase are both not statistically independent and not additive, the subtraction of systematic effects, such as those treated in this paper, requires the use of Stokes parameters, which are statistically independent. Second, we are interested in applying the correction as early as possible in the processing of the data, even at the level of the single event before polarization determination, to leave greater flexibility in the subsequent analysis. For these reasons, we deemed it more appropriate not to follow the classical approach, but instead to start from the Stokes parameters of the single events.

The approach used in this paper to compute polarization is derived from Kislat et al. (2015), with the minor difference of a factor of 2 in the definition of the Stokes parameters. For each photon with photoelectric position angle  $\phi_i$ , the  $q_i$  and  $u_i$  Stokes parameters are computed

$$q_i = 2 \cos(2\phi_i) \quad (2)$$

$$u_i = 2 \sin(2\phi_i). \quad (3)$$

Each event has a known spatial position and spectral energy. The events are therefore selected inside the range desired, and for the  $N$  selected events, the normalized  $q$  and  $u$  Stokes



**Figure 2.** Modulation curves for polarized (left), unpolarized at 5.9 keV (upper right), and unpolarized at 2.3 keV (bottom right) radiation. For polarized radiation, a modulation is seen, which is absent for unpolarized radiation at high energies but reappears at low energies as spurious modulation.

parameters are computed:

$$q = \frac{\sum_i q_i}{N} \quad (4)$$

$$u = \frac{\sum_i u_i}{N}, \quad (5)$$

with uncertainty given by the standard deviation

$$\sigma_q = \sqrt{\frac{2-q^2}{N-1}} \quad (6)$$

$$\sigma_u = \sqrt{\frac{2-u^2}{N-1}}. \quad (7)$$

From these, the modulation can be obtained:

$$m = \sqrt{q^2 + u^2}. \quad (8)$$

The polarization degree is then given by Equation (1), while the polarization position angle is given by

$$\varphi = \frac{1}{2} \tan^{-1} \left( \frac{u}{q} \right). \quad (9)$$

While the Stokes parameters ( $q$ ,  $u$ ) have statistical uncertainties ( $\sigma_q$ ,  $\sigma_u$ ) that are Gaussian-distributed and uncorrelated, the modulation and position angle ( $m$ ,  $\varphi$ ) do not. However, for measurements of high statistical significance, the uncertainties ( $\sigma_m$ ,  $\sigma_\varphi$ ) become approximately Gaussian distributed and uncorrelated, with

$$\sigma_m \approx \sqrt{\frac{2-m^2}{N-1}} \quad (10)$$

and

$$\sigma_\varphi \approx \frac{1}{m\sqrt{2(N-1)}} \quad (11)$$

for  $m/\sigma_m \gg 1$ .

These uncertainties are valid without the application of the systematic corrections described in this paper, but represent nonetheless a good approximation for celestial observations of high statistical significance. The complete expressions are described below in Section 4.3, where the corrected Stokes parameters of any systematic effects are simply taken into account.

## 2.2. Systematic Effects

For unpolarized radiation, an ideal polarimeter would measure only a very small amplitude of modulation due to the Poisson distribution of photoelectrons and decreasing as the number of counts increases; however, this is not found to be the case with the GPD, in which a systematic signal, called spurious modulation, is detectable.

Figure 2 shows the impact of spurious modulation: For polarized radiation (left), a clear modulation is seen, which is absent for unpolarized radiation at high energies (upper right), for which a curve very close to flat is seen. However, for unpolarized radiation at lower energies (bottom right), a modulated component appears as spurious modulation.

It should be noted that spurious modulation behaves essentially as an additional  $\cos^2$  contribution, i.e., it has the same frequency as the modulation caused by a genuine source polarization. As a consequence, the sum of genuine and spurious modulation will still be a  $\cos^2$ . For this reason, and depending on the phase, spurious modulation might appear “hidden” from the polarized modulation curve, but is actually present, changing the measured modulation and shifting the observed phase.

As presented by F. Muleri et al. (2021, in preparation), spurious modulation is constant within the calibration requirements of 0.3% over variations in time, temperature, and source rate; as a consequence, ground calibration measurements can be used to correct flight data. The same paper presents the quantitative details regarding the effect of spurious modulation

on IXPE observations, given the actual calibration measurements available for each detector unit of IXPE.

### 2.3. Statistical Treatment in the Presence of Systematic Effects

In this section, the formalism of Kislat et al. (2015) to compute expected values and variances is extended to include spurious modulation, evaluating the case of a second component in the polarimetric signal.

The probability distribution function for the photoelectron emission angles in the case of an ideal X-ray polarimeter is given by

$$f(\varphi) = \frac{1}{2\pi} [1 + \mu p_0 \cos(2(\varphi - \varphi_0))]. \quad (12)$$

Considering the  $q_i$  and  $u_i$  Stokes parameters values for a single event (Equations (2) and (3)), the expected values for the Stokes parameters  $q_0$  and  $u_0$  can be estimated by the relations

$$E[q_0] = \int_0^{2\pi} f(\varphi) 2 \cos(2\varphi) d\varphi = \mu p_0 \cos(2\varphi_0) \quad (13)$$

$$E[u_0] = \int_0^{2\pi} f(\varphi) 2 \sin(2\varphi) d\varphi = \mu p_0 \sin(2\varphi_0). \quad (14)$$

In the same way, the variances can be evaluated

$$\begin{aligned} \text{Var}[q_0] &= \int_0^{2\pi} f(\varphi) (2 \cos(2\varphi) - E[q_0])^2 d\varphi \\ &= 2 - (\mu p_0 \cos(2\varphi_0))^2 = 2 - E[q_0]^2 \end{aligned} \quad (15)$$

$$\begin{aligned} \text{Var}[u_0] &= \int_0^{2\pi} f(\varphi) (2 \sin(2\varphi) - E[u_0])^2 d\varphi \\ &= 2 - (\mu p_0 \sin(2\varphi_0))^2 = 2 - E[u_0]^2. \end{aligned} \quad (16)$$

To extend this approach to take into account a second  $\cos^2(\varphi)$  component, as expected for spurious modulation, we can define a new probability distribution function:

$$g(\varphi) = \epsilon_{\text{sm}} \cos(2(\varphi - \varphi_{\text{sm}})), \quad (17)$$

where  $\epsilon_{\text{sm}}$  and  $\varphi_{\text{sm}}$  are respectively the amplitude and phase of spurious modulation. The new overall probability distribution function is

$$F(\varphi) = \frac{1}{2\pi} [2\pi f(\varphi) + g(\varphi)]. \quad (18)$$

From this distribution, the new expected values for  $q$  and  $u$  are obtained:

$$\begin{aligned} E[q] &= \int_0^{2\pi} F(\varphi) 2 \cos(2\varphi) d\varphi \\ &= E[q_0] + \epsilon_{\text{sm}} \cos(2\varphi_{\text{sm}}) = E[q_0] + E[q_{\text{sm}}] \end{aligned} \quad (19)$$

$$\begin{aligned} E[u] &= \int_0^{2\pi} F(\varphi) 2 \sin(2\varphi) d\varphi \\ &= E[u_0] + \epsilon_{\text{sm}} \sin(2\varphi_{\text{sm}}) = E[u_0] + E[u_{\text{sm}}]. \end{aligned} \quad (20)$$

These results show that spurious modulation is an additional summative term to the expected value, and therefore can be subtracted:

$$q_{\text{corr}} = q_{\text{meas}} - q_{\text{sm}} \quad (21)$$

$$u_{\text{corr}} = u_{\text{meas}} - u_{\text{sm}}. \quad (22)$$

Moreover, the same approach allows to obtain the variance in the presence of spurious modulation:

$$\begin{aligned} \text{Var}[q] &= \int_0^{2\pi} F(\varphi) (2 \cos(2\varphi) - E[q])^2 d\varphi \\ &= \text{Var}[q_0] - (2\mu p_0 \epsilon_{\text{sm}} \cos(2\varphi_0) \cos(2\varphi_{\text{sm}}) + \epsilon_{\text{sm}}^2 \cos^2(2\varphi_{\text{sm}})) \\ &= \text{Var}[q_0] - \text{Var}[q_{\text{sp}}] \end{aligned} \quad (23)$$

$$\begin{aligned} \text{Var}[u] &= \int_0^{2\pi} F(\varphi) (2 \sin(2\varphi) - E[u])^2 d\varphi \\ &= \text{Var}[u_0] - (2\mu p_0 \epsilon_{\text{sm}} \sin(2\varphi_0) \sin(2\varphi_{\text{sm}}) + \epsilon_{\text{sm}}^2 \sin^2(2\varphi_{\text{sm}})) \\ &= \text{Var}[u_0] - \text{Var}[u_{\text{sp}}], \end{aligned} \quad (24)$$

where the terms

$$\text{Var}[q_{\text{sp}}] = 2\mu p_0 \epsilon_{\text{sm}} \cos(2\varphi_0) \cos(2\varphi_{\text{sm}}) + \epsilon_{\text{sm}}^2 \cos^2(2\varphi_{\text{sm}}) \quad (25)$$

$$\text{Var}[u_{\text{sp}}] = 2\mu p_0 \epsilon_{\text{sm}} \sin(2\varphi_0) \sin(2\varphi_{\text{sm}}) + \epsilon_{\text{sm}}^2 \sin^2(2\varphi_{\text{sm}}) \quad (26)$$

take into account the variance due to the presence of spurious modulation.

It is worth noting that, in all practical situations, the first term ( $\text{Var}[q_0]$  and  $\text{Var}[u_0]$  of Equations (15) and (16)) is much larger than the second ( $\text{Var}[q_{\text{sp}}]$  and  $\text{Var}[u_{\text{sp}}]$ ), which can be neglected. In fact, even in the worst-case scenario of a large source polarization ( $\mu p_0 \approx 0.2$ ) and large spurious modulation ( $\epsilon_{\text{sm}} \approx 0.05$ ), which maximizes the latter contribution, the first term in Equations (23) and (24) is  $\approx 2$ , whereas the second is  $\approx 0.006$ .

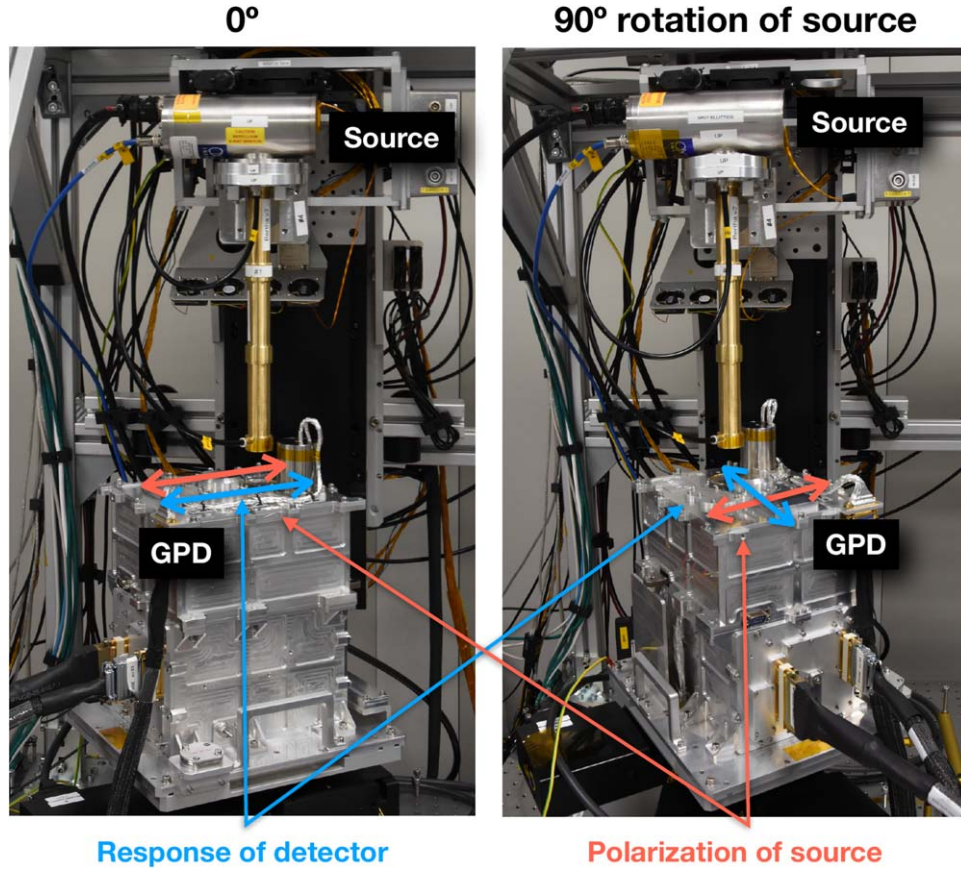
### 3. Measurement of the Response to Unpolarized Radiation

In this section, we describe the method used to measure spurious modulation. The laboratory sources used to do this measurement are partially polarized, with the exact degree of polarization depending on a number of parameters that are difficult to estimate, such as the geometry of the emission internal to the source and the source spectrum (see Muleri et al. (2022)). Therefore, we define a procedure to decouple the intrinsic response of the instrument from the signal due to any genuine source polarization, which is based on repeating the measurement at two polarization angles shifted of  $90^\circ$ . For these two measurements, from the GPD reference frame, the angle of spurious modulation remains constant, while the angle of the intrinsic modulation of the source changes by  $90^\circ$  (see Figure 3). Therefore, the modulation caused by the true source polarization and the spurious one will sum differently in the two measurements.

Starting from the normalized Stokes parameters  $q$  and  $u$  (Equations (4) and (5)), for the two measurements we have

$$\begin{cases} q_0 = q_{\text{sm}} + q_{\text{source}}(\epsilon = 0^\circ) \\ q_{90} = q_{\text{sm}} + q_{\text{source}}(\epsilon = 90^\circ) = q_{\text{sm}} - q_{\text{source}}(\epsilon = 0^\circ) \end{cases} \quad (27)$$

$$\begin{cases} u_0 = u_{\text{sm}} + u_{\text{source}}(\epsilon = 0^\circ) \\ u_{90} = u_{\text{sm}} + u_{\text{source}}(\epsilon = 90^\circ) = u_{\text{sm}} - u_{\text{source}}(\epsilon = 0^\circ) \end{cases} \quad (28)$$



**Figure 3.** Rotation of the source to decouple the contribution to polarization due to spurious modulation and due to the polarization of the source. A rotation of  $90^\circ$ , from the point of view of the detector, changes the sign of the Stokes parameters of the source but not of spurious modulation. For this reason, all calibration measurements are taken at two orthogonal rotation angles.

where *sm* refers to the contribution of spurious modulation (independent from the rotation angle), and *source* refers to the contribution due to the source (dependent on the rotation angle). The change of sign of the source components after a  $90^\circ$  rotation is due to the fact that  $q$  is defined as  $q = 2 \cos(2\phi)$  and analogously  $u$  (Equations (2) and (3)). Solving the system of equations above gives

$$q_{sm} = \frac{q_0 + q_{90}}{2} \quad (29)$$

$$u_{sm} = \frac{u_0 + u_{90}}{2}, \quad (30)$$

with uncertainty given by

$$\sigma_{q_{sm}} = \frac{1}{2} \sqrt{\sigma_{q_0}^2 + \sigma_{q_{90}}^2} = \frac{1}{2} \sqrt{\frac{2 - q_0^2}{N_0 - 1} + \frac{2 - q_{90}^2}{N_{90} - 1}} \quad (31)$$

$$\sigma_{u_{sm}} = \frac{1}{2} \sqrt{\sigma_{u_0}^2 + \sigma_{u_{90}}^2} = \frac{1}{2} \sqrt{\frac{2 - u_0^2}{N_0 - 1} + \frac{2 - u_{90}^2}{N_{90} - 1}}. \quad (32)$$

Analogously, it is possible to obtain the Stokes parameters of the source  $q_{source}$  and  $u_{source}$  as a byproduct of this method:

$$q_{source} = \frac{q_0 - q_{90}}{2} \quad (33)$$

$$u_{source} = \frac{u_0 - u_{90}}{2}. \quad (34)$$

These equations will be used as a comparison to test the correction algorithm below in Section 5.

The correction can be applied by subtracting from a measurement the spurious modulation calculated with Equations (29) and (30).

However, this has two disadvantages:

1. GPD spurious modulation is position-dependent (Baldini et al. 2021), and therefore photons used for calibration should be extracted from the same region as that for measurement. This is very impractical.
2. If the photons selected have a nonmonochromatic spectrum, the correction cannot easily take into account the energy dependence of spurious modulation.

These two problems can be overcome by correcting each event (i.e., each photon) individually. This method, which is the one that will be used for celestial observations, is described in the next section.

## 4. Description of the Photon-by-photon Algorithm

### 4.1. Creation of the Calibration Database

The creation of the calibration database is based on measurements illuminating the entire GPD sensitive area (flat-field measurement), repeated at two source azimuthal angles, one orthogonal with respect to the other, and at different energies.

For each energy and angle, the events are divided, according to their spatial positions (track estimated absorption points), in

a certain number of bins ( $300 \times 300$  in this paper). In each spatial bin, the normalized Stokes parameters are computed from Equations (4) and (5). The Stokes parameters for spurious modulation for each bin are then computed from Equations (29) and (30). These matrices are saved in a file, which also contains the energy for each map. Examples of these maps are shown in Figure 4.

The number of bins is chosen so as to have sufficient granularity in the source image. However, it should be noted that the correction of the single event is by itself not significant, but the correction over many events becomes statistically functional.

#### 4.2. Spurious Modulation Removal

A measurement is corrected photon by photon, subtracting from the Stokes parameters of the event the values measured during calibration in the spatial bin in which the photon is absorbed and at its measured energy. To achieve this last point, Stokes maps at different energies are linearly interpolated bin by bin.

In practice, Equations (2) and (3) are modified as

$$q[i]_{\text{uncorrected}} = 2 \cos(2\phi[i]) \quad (35)$$

$$u[i]_{\text{uncorrected}} = 2 \sin(2\phi[i]) \quad (36)$$

$$q[i]_{\text{corrected}} = q[i]_{\text{uncorrected}} - q_{\text{sm}}[\text{bin}_x][\text{bin}_y][\text{energy}] \quad (37)$$

$$u[i]_{\text{corrected}} = u[i]_{\text{uncorrected}} - u_{\text{sm}}[\text{bin}_x][\text{bin}_y][\text{energy}], \quad (38)$$

where  $q_{\text{sm}}$  and  $u_{\text{sm}}$  are the values of the maps created in Section 4.1.

The Stokes parameters for all events under consideration are then given by Equations (4) and (5), and the modulation, polarization, and phase are given by Equations (8), (1), and (9), respectively.

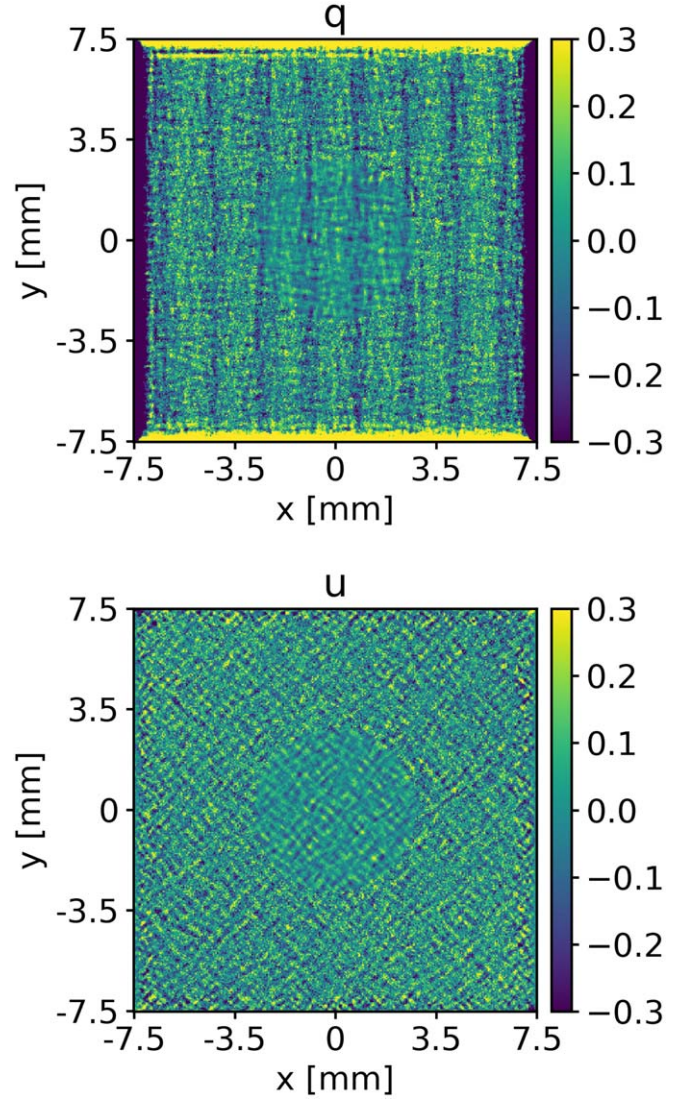
#### 4.3. Uncertainty on Calibrated Modulation

To understand how the uncertainties propagate, it can be instructive to write the expression for the corrected normalized  $q$  parameter including Equations (37) in (4) (the  $u$  case is analogous)

$$q_{\text{corrected}} = \frac{\sum_i [q_{\text{unc},i}(x_i, y_i, E_i) - q_{\text{sm}}(\text{bin}_x, \text{bin}_y, \text{bin}_E, E_i)]}{N_{\text{obs}}}, \quad (39)$$

where it is evident that each uncorrected event of the observation depends on the spatial position  $x_i, y_i$  and on the measured energy  $E_i$ , while the subtracted spurious modulation depends on the bins (both the spatial and energy calibration bins) and on the specific interpolated energy  $E_i$  inside the bin.  $N_{\text{obs}}$  is the number of events in the observation, which should be distinguished from the number of events in the calibration measurements. The expression above can be expanded by separating the sum over the spatial and energy bins  $\sum_{\text{bins}}$  from the sum over the single events inside each bin  $\sum_j$ :

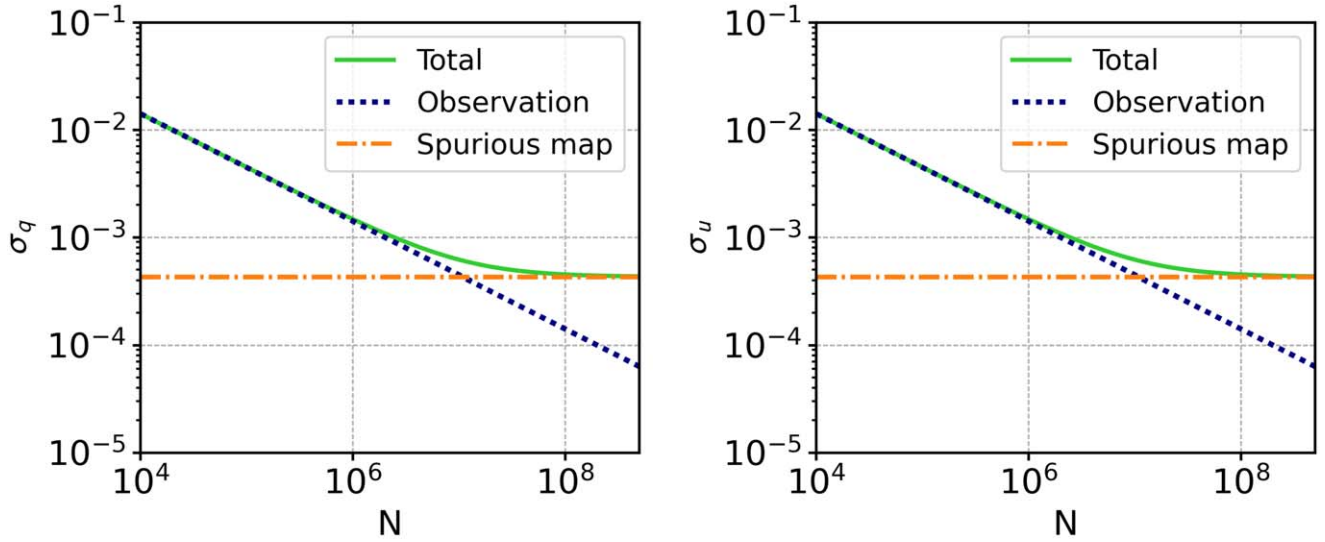
$$q_{\text{corrected}} = \frac{\sum_i q_{\text{unc},i}(x_i, y_i, E_i)}{N_{\text{obs}}} - \frac{\sum_{\text{bins}} \left[ \sum_j q_{\text{sm}}(\text{bin}_x, \text{bin}_y, \text{bin}_E, E_j) \right]}{N_{\text{obs}}}. \quad (40)$$



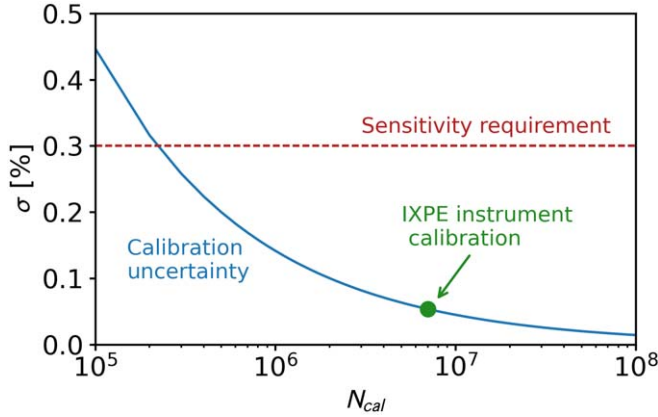
**Figure 4.** Examples of spurious modulation maps for Stokes parameters  $q$  and  $u$  at 2.7 keV. The central region is smoother because it was calibrated with a larger statistics. It is also worth noting that values at the border are biased because photoelectric tracks are truncated by the physical size of the ASIC used for reading out the signal. The bias is such that the angle is biased to  $90^\circ$  for vertical edges and to  $0^\circ$  for horizontal edges.  $q$  is defined as the cosine of twice such angle (Equation (2)), and therefore, values are biased to  $\sim \cos(2 \cdot 90^\circ)$  and  $\sim \cos(2 \cdot 0^\circ)$ .  $u$  (Equation (3)), instead, is  $\sim \sin(2 \cdot 90^\circ)$  and  $\sim \sin(2 \cdot 0^\circ)$ , and therefore the bias is around 0.

It should be noted that  $\sum_{\text{bins}}$  is a sum over uncorrelated terms, while  $\sum_j$  is a sum over (partially) correlated terms (this is because the subtracted spurious modulation comes from the same bin). Looking at the uncertainty and (as a worst case) assuming correlation = 1 in the same spatial and energy bins,  $\sum_j$  disappears and one uncertainty is considered for each bin (this is a good approximation because the variation with energy due to interpolation in the same energy bin is small). The total uncertainty is

$$\sigma_{q_{\text{corrected}}} = \sqrt{\sigma_{q_{\text{unc}}}^2 + \sum_{\text{bins}} \left( \frac{n_{\text{obs}}(\text{bin}_x, \text{bin}_y, \text{bin}_E)}{N_{\text{obs}}} \sigma_{q_{\text{sm}}}(\text{bin}_x, \text{bin}_y, \text{bin}_E) \right)^2}, \quad (41)$$



**Figure 5.** Comparison of the first term (Observation) and second term (Spurious map) of the uncertainty expression (Equation (41)) as a function of the number of events of the observation. It can be seen that the second term is often negligible. Also plotted is the total quadratic sum of the two terms, which tends to an asymptotic value that is the residual due only to calibration. This example is at 2.7 keV with  $7 \cdot 10^6$  events in the spurious modulation map.



**Figure 6.** Uncertainty on modulation, as a function of the number of counts  $N_{cal}$  in the calibration measurements, for the ideal case of an infinite number of counts in the observation. The uncertainty in this case depends on the number of counts in the calibration measurement as  $\sigma \approx \sqrt{2/N_{cal}}$ . Also shown in this plot are the IXPE requirement of 0.3% modulation and the number of counts of IXPE’s calibration measurement (at 2.7 keV but representative of the other energies).

where  $\sigma_{unc}$  is given by Equation (6),  $\sigma_{q_{sm}}$  is given by Equation (31), and  $n_{obs}$  is the sum of the events of the observation in the spatial and energy bins. The two terms are compared in Figure 5, where it can be seen that the second term will be negligible in most practical situations, as IXPE observations will typically have a number of counts smaller than calibrations. In this case, the simpler expressions of Equations (6), (7), (10), and (11) can be used. The two terms are also further compared using simulations in Section 5.5.

The same plot also presents the quadratic sum of the two terms. It can be seen that the uncertainty value tends to an asymptotic value, which is the residual uncertainty due only to calibration.

To understand what this minimum uncertainty (proportional to the minimum detectable amplitude) is, we can consider the ideal case of an infinite number of counts in the observation. In this ideal scenario, the uncertainty on a modulation

measurement depends only on the number of counts  $N_{cal}$  in the calibration measurements. For IXPE’s GPDs, in which spurious modulation is not too high, Equation (10) can be approximated as  $\sigma \approx \sqrt{2/N_{cal}}$ . This last expression also gives the same result as the II term of Equation (41) if the observation is spatially uniform and monochromatic. This uncertainty is plotted in Figure 6, where it is shown that IXPE’s instrument calibration has been made with enough counts to be well inside the requirement. The actual sensitivity will be worse than this estimate because of small temporal variations, but still well inside the requirement (F. Muleri et al. 2021, in preparation).

## 5. Testing the Spurious Modulation Correction

### 5.1. Modulation of Monochromatic Laboratory Sources

To test the effectiveness of the correction, we compare some results of on-ground calibration obtained with the photon-by-photon algorithm described in Section 4, with the results of the “standard” analysis described in Section 3, here named global decoupling.

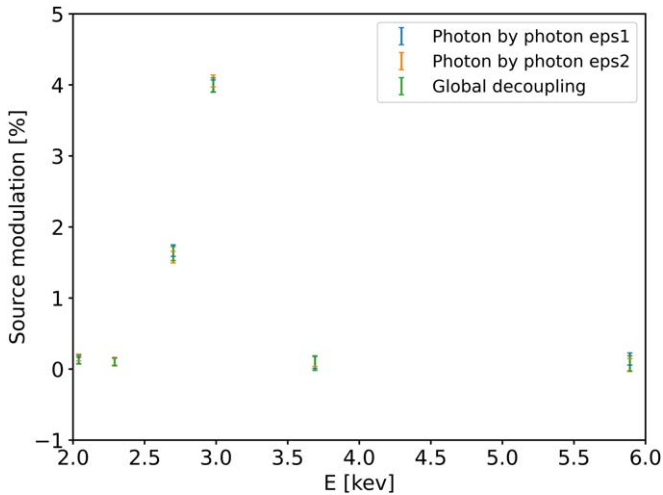
We show in Figure 7 the modulation due to the genuine polarization of the sources used for the calibration of IXPE DUs, derived as byproduct of the calibration of the detector response to unpolarized radiation. One value is referred to the global decoupling; the other two values are the application of the photon-by-photon algorithm to the two measurements rotated of 90 degrees (hence the two values). All three values are compatible.

In Figure 8, we compare the value of modulation factor, measured with polarized sources, obtained with the two different methods. All three values are again compatible.

These tests prove that, for monochromatic sources, the photon-by-photon correction method retrieves the correct modulation.

### 5.2. Spectrally Resolved Polarization

One of the sources used for ground calibration is the Ca X-ray tube, whose spectrum comprises of calcium fluorescence lines plus a significant contribution from continuum



**Figure 7.** Modulation of low-polarization flat-field laboratory sources at various energies. One value is referred to the global decoupling; the other two values are the application of the photon-by-photon algorithm to the flat fields at the two rotation angles (named *eps1* and *eps2*) at which this measurement was acquired (hence the two values). All three values are compatible.

bremsstrahlung emission. This source is expected to be completely unpolarized from first principles (see Muleri et al. 2022), and also offers an opportunity to test the algorithm for spurious modulation removal with nonmonochromatic sources. In this case, it is necessary to correct for spurious modulation each single photon with its specific measured energy, as is done by the photon-by-photon algorithm. The Stokes parameters and subsequent modulation can then be obtained for photons in different energy bins.

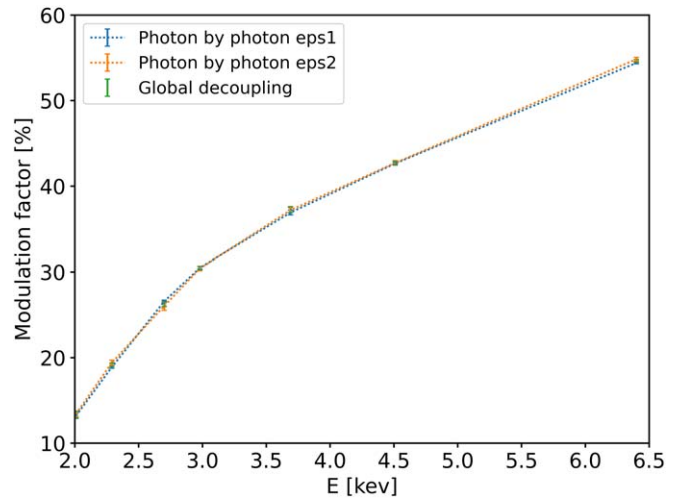
This is shown in Figure 9. The colored data points are corrected for spurious modulation, and are compatible with 0 as expected, while the gray points are the uncorrected points.

Two points should be noted from this result. First, this is a situation in which only the photon-by-photon algorithm can be used, which therefore demonstrates its more general applicability. Second, the uncorrected points show a slightly decreasing trend (a consequence of the fact that spurious modulation decreases with energy; see Muleri et al. (2021, in preparation)); this trend disappears after correction, proving that the algorithm is removing the systematic effect correctly.

### 5.3. Effect of Finite Energy Resolution

The GPD, like any other real detector, measures the energy of the event with a finite energy resolution. Spurious modulation changes with the true energy of the radiation, but is corrected starting from the *measured* energy. In this section, we evaluate the effect, if any, for a representative observation simulated with the detailed GPD Monte Carlo software developed by the IXPE team (L. Baldini et al. 2021, in preparation).

The simulation proceeds as follows. The first step is to input a Crab-like spectrum (a power law with index 2) in the Monte Carlo to produce photoelectron track images equivalent to those obtained with real measurements with the GPD. These are reprocessed with the same software used for real data. Simulations are able to reproduce all the characteristics of a real measurement in fine detail, with the exception of spurious modulation. Such a component is added event by event, interpolating the maps of spurious modulation (obtained with



**Figure 8.** Same as Figure 7, but for the modulation factor (obtained by dividing the source modulation of the polarized measurements by the source polarization, as in Equation (1)).

calibration) at the true photon energy provided by the Monte Carlo. In the following step, spurious modulation is subtracted but its value is obtained by interpolating the calibration maps at the measured energy.

The measured modulation is compared with the expected value in Figure 10. The latter is derived by processing the data obtained from the Monte Carlo without adding (and removing) spurious modulation. It is evident that the two values agree very well. The comparison of the source spectrum in true and measured energy is shown in the same figure.

### 5.4. Spatial Uniformity of the Correction

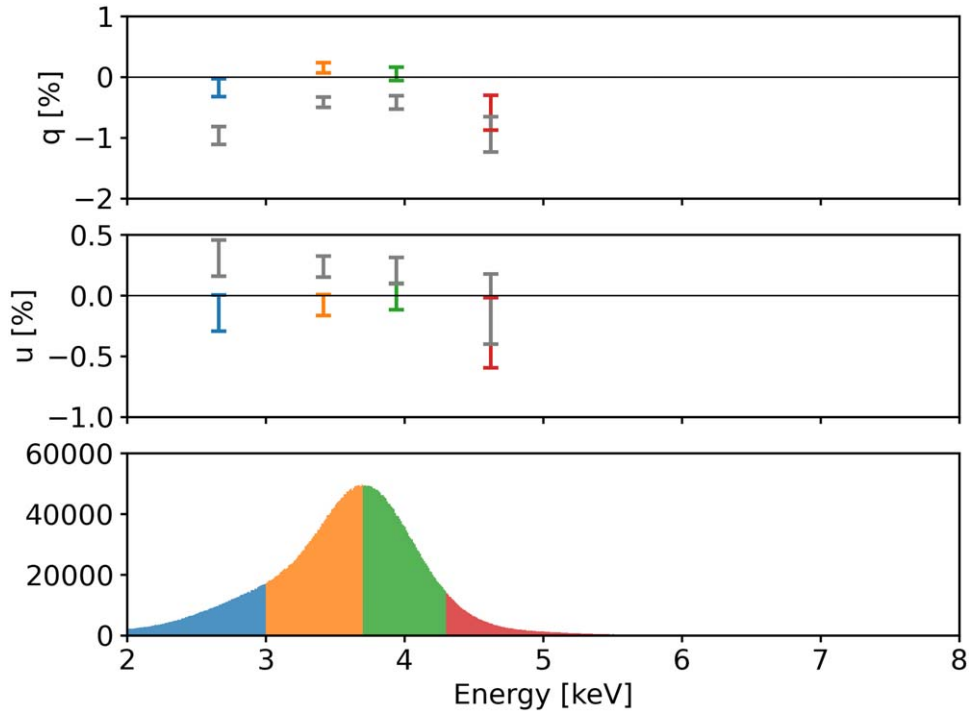
The GPD is a detector with imaging capabilities, and therefore the correction algorithm will be applied in different parts of the detector, and also in regions of different sizes. To verify the spatial uniformity of the correction, the comparison between the correction algorithm and the standard analysis (global decoupling), as done in Section 5.1, was repeated for the measurement at 2.7 keV, in spatial regions of different position and size. As can be seen in Figure 11, the algorithm performs well the corrections over the entire detector.

### 5.5. Simulations

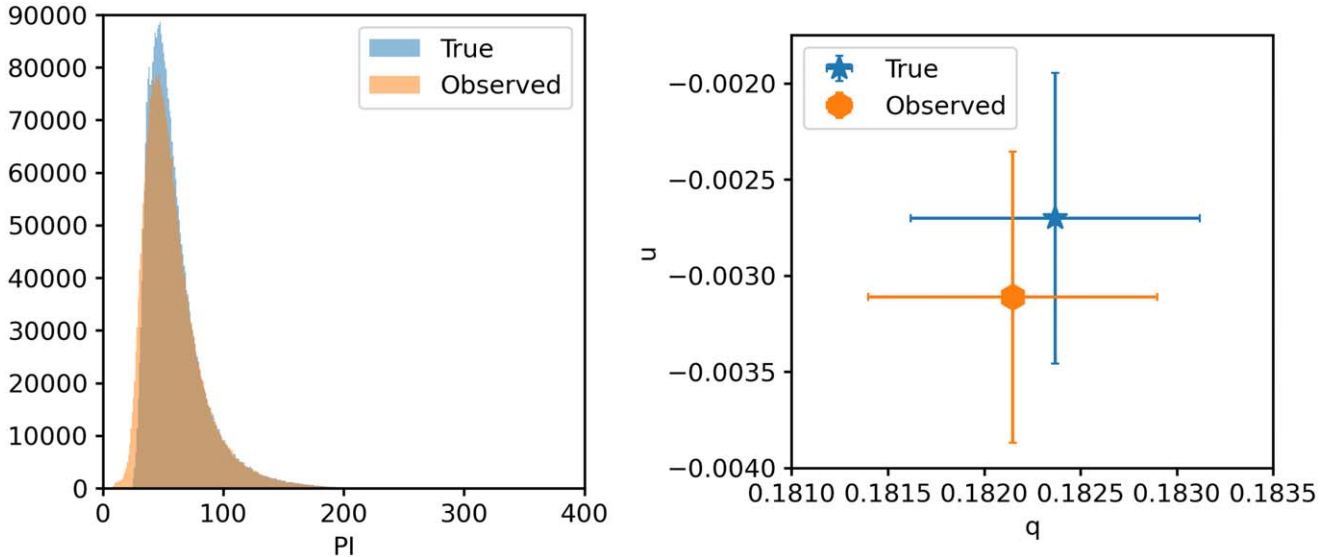
To further test the statistical distribution of the calibrated measurements, we simulated the application of spurious modulation calibrations to toy observations. Both the calibration measurements and monochromatic observations (see precise definitions below) were simulated, mimicking the process that will be used in reality. To each observation, a spurious modulation (dependent only on energy) is added (and then removed using the simulated calibrations). The goal of these simulations is to prove that, by subtracting the calibration measurements from the observations, the true modulation value is retrieved with the correct uncertainty as calculated in Equation (41).

#### 5.5.1. Simulation Procedure

We define two types of simulated measurements:



**Figure 9.** Spectra of the Ca X-ray tube with the modulation computed in energy bins. The colored points are corrected for spurious modulation using the photon-by-photon correction which therefore is sensitive to the different energies), while the gray points are uncorrected. The corrected points are compatible with 0 as expected for the Ca X-ray tube, while for the uncorrected points, the decreasing trend of spurious modulation with energy is evident.



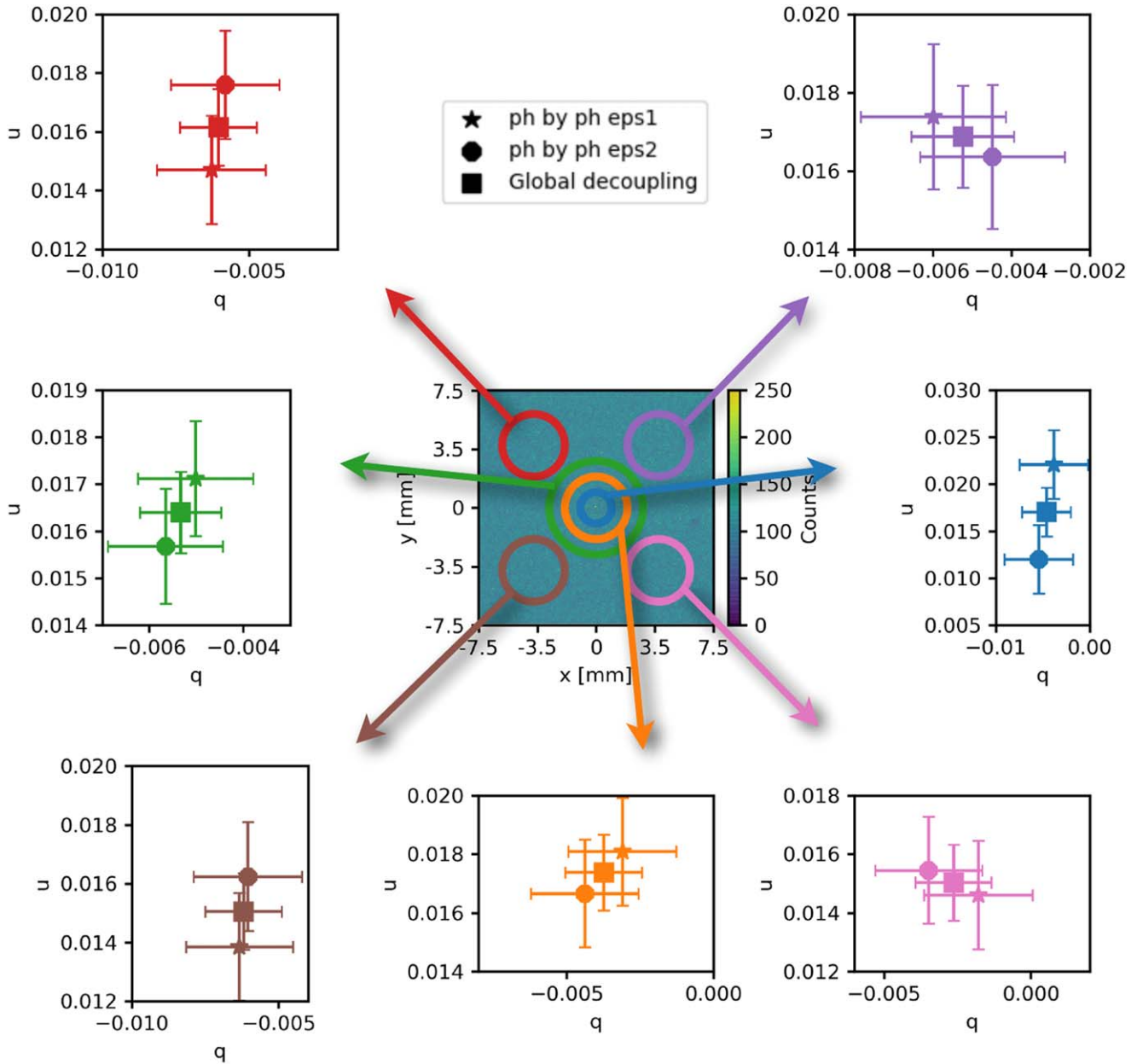
**Figure 10.** Comparison of modulation corrected using the true and observed energy using a 3.5M event Monte Carlo simulation of a Crab-like spectrum. The plot on the left compares the spectra, and the one on the right the Stokes parameters of the observation. Spurious modulation is first summed by interpolating the calibration maps using the true energy (given in input to the Monte Carlo), and then subtracted by interpolating using the measured energy. As can be seen, the offset in the correction due to the discrepancy between the two energy estimates is negligible.

1. “Calibration”—simulated calibration measurement analogous to the ground measurements carried out to calibrate the response of the IXPE detectors. In the following, we focus the discussion only on a subrange of the energy range that was effectively calibrated, i.e., we simulated just two measurements at 2.7 and 2.98 keV.

Analogously to real measurements, we simulated two measurements at orthogonal angles, each consisting of

$15 \times 10^6$  events at 2.7 and 2.98 keV and characterized by a polarization equal to the measured one. From these measurements, spurious modulation is derived as described in Section 3, with an uncertainty given by Equations (31) and (32) (see details below).

2. “Observation”—simulated IXPE observation of a (toy) celestial source. In the following, we assume that the source is monochromatic, with energy between 2.7 and



**Figure 11.** Modulation generated by the genuine source polarization at 2.7 keV, obtained by correcting spurious modulation with different methods in several regions of the detector. One value is referred to the global decoupling; the other two values are the application of the photon-by-photon algorithm to the flat fields at the two rotation angles (named *eps1* and *eps2*) at which this measurement was acquired (hence the two values). All three values are compatible over all the detectors, showing that the correction algorithm performs the same in different regions of the detector and/or with different extraction radii.

2.98 keV, and that its true polarization is  $q = 0.04$  and  $u = 0.02$ , which is representative of the weakly polarized sources that will be observed by IXPE.

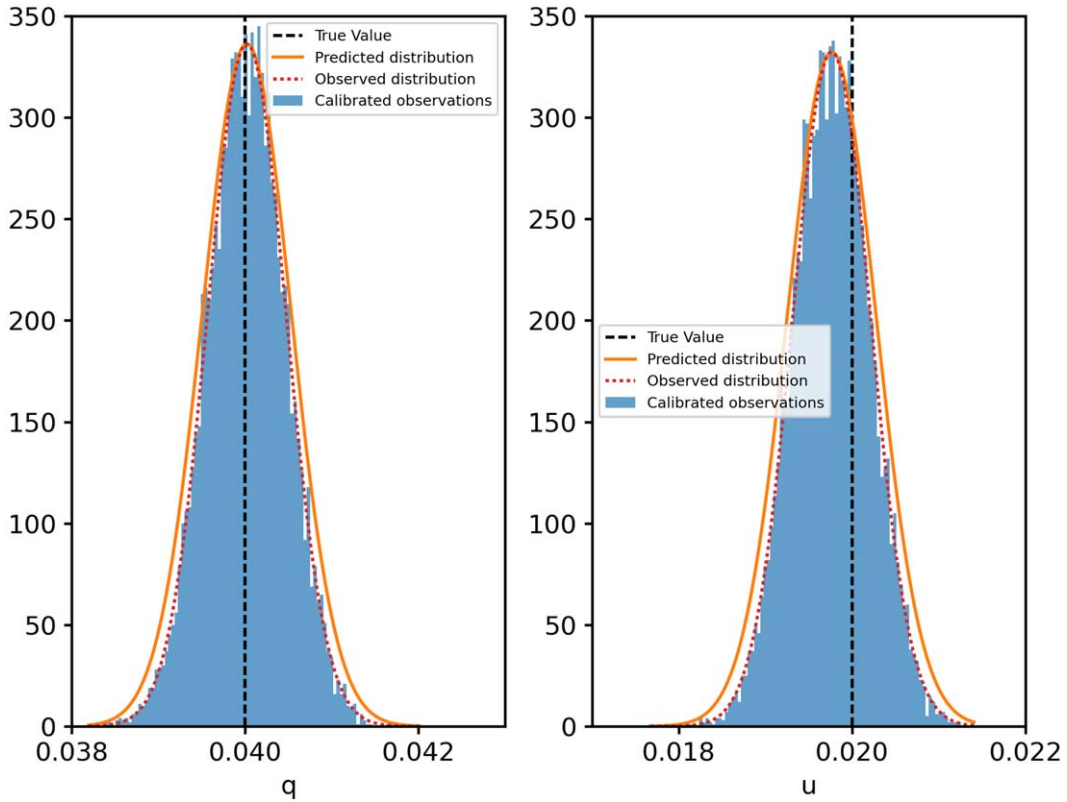
A simulated measurement, either for calibration or toy observation, is generated assuming a distribution of the photoelectric position angles obtained from a  $\cos^2$  distribution with the desired modulation and phase, and an energy obtained from a Gaussian distribution with width given by the approximate real energy resolution of the detector

Each simulated measurement is a list of events, each consisting of its Stokes parameters and energy. To the Stokes parameters, a toy spurious modulation is summed, derived by phenomenologically fitting the real dependence as the inverse of energy.

The observations (second point above) are then corrected, using the calibration measurements (first point), by applying the photon-by-photon subtraction method described in this paper.

#### 5.5.2. Distribution of Observations with One Calibration Data Set

We first investigated the case of the statistical distribution of the polarization obtained by a corrected observation at energy  $E = 2.8$  keV in the case where only one calibration data set is available, which is the real case. Here,  $10^4$  observations with  $10^7$  events each were simulated and corrected (using the same calibration data set for all). In this case, the uncertainty on calibration measurements (second term of Equation (41)) is comparable with the statistical uncertainty on observations



**Figure 12.** Observation at 2.8 keV consisting of  $10^4$  iterations with  $10^7$  events in each iteration. The predicted distribution of the observed values (orange line) is compared with the fit to the observed distribution (red line). The former has a larger width, because it accounts for the fact that, in correcting, we are subtracting an estimate of spurious modulation and not its true value. This causes a shift between the true modulation (vertical line) and the center of the observed distribution.

(first term of Equation (41)), but this will not be the case in most practical situations.

The distribution of the derived source polarization is shown in Figure 12. While values are Gaussian-distributed with a width derived from the number of counts in the observation as expected, the average value is shifted (this is particularly evident for  $u$ ). This shift is due to the fact that we subtracted an *estimate* of the spurious modulation amplitude and not its *true* value. As we will see in the following, the second term in Equation (41) accounts for this quite well.

In most IXPE observations, the number of events will be much smaller than the number of calibration events. In this case, the uncertainty on calibration measurements is negligible compared with the statistical uncertainty on the observations, and so the difference between the estimated and true value of subtracted spurious modulation will also be negligible. In this assumption, the observed and predicted distributions would be essentially coincident.

### 5.5.3. Distribution of Observations with Many Calibration Data Sets

In the previous section, we have seen that corrected observations have a (small) offset with respect to the true value. We associated such a difference with the fact that we can remove from the observation just an estimate of the spurious modulation derived from calibration, and not its true value. To substantiate this claim, we investigate the observed values when the observations are corrected with many independent calibrations, which are then statistically distributed around the true value.

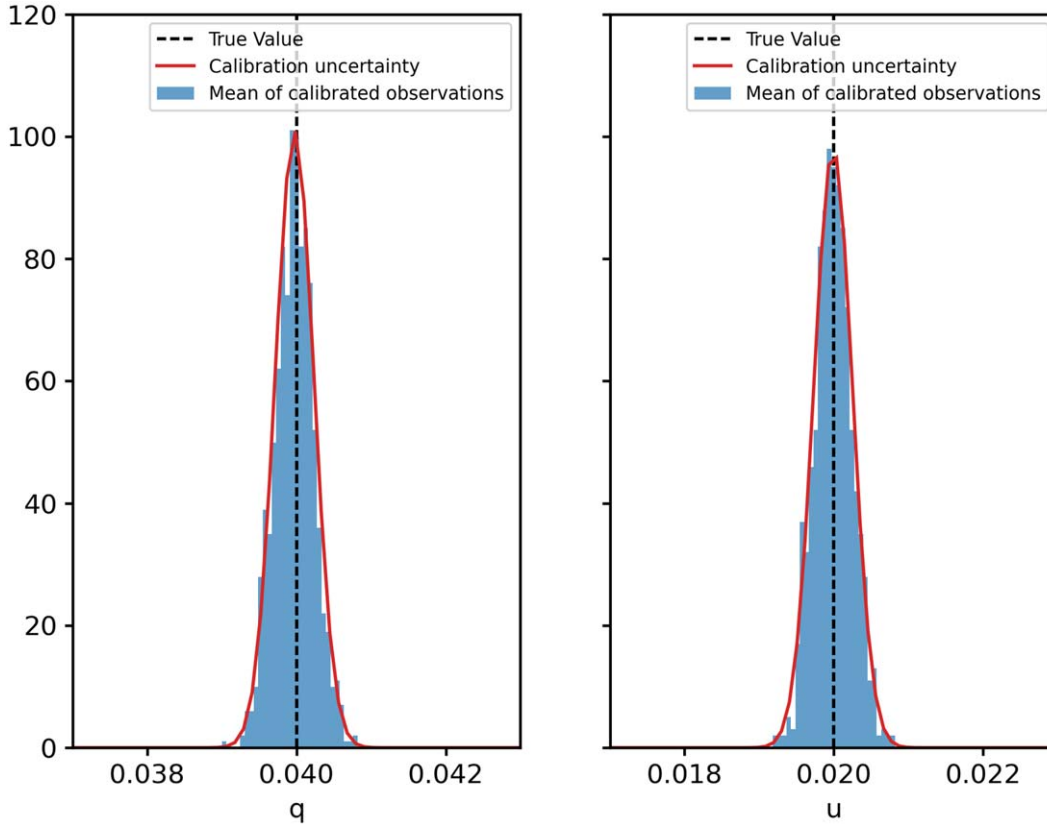
To study this,  $10^4$  observations with  $10^6$  events each were again simulated (numbers chosen to keep the simulation running time reasonable). This time, however, each of these was corrected using  $10^3$  different calibration measurements, i.e., it was corrected  $10^3$  times. All of this was repeated at 2.7 keV and 2.98 keV (the calibration energies) and at other intermediate energies in the chosen 2.7–2.98 keV energy range.

Each of the  $10^3$  sets of calibrated observations was fitted to derive the center of the observed source polarization for the different calibrations. The distribution of such values is shown in Figure 13.

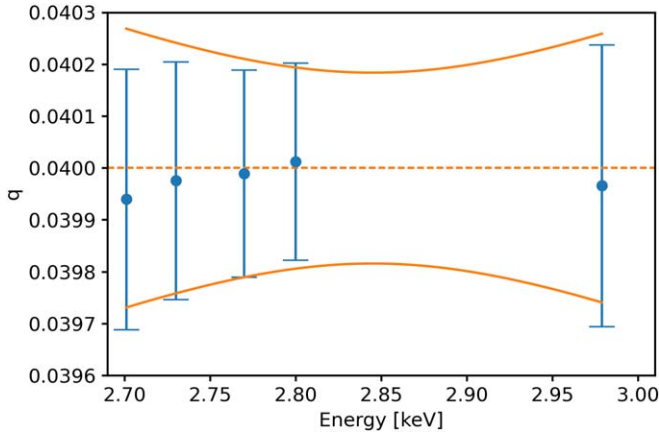
The distribution is centered on the true modulation of the source. This was expected because, averaging many independent calibrations, the value of spurious modulation that is corrected will tend to the true value. However, the width of the distribution varies. The fitted standard deviation of the distributions is 0.026% at 2.7 keV, 0.023% at 2.73 keV, 0.021% at 2.77 keV, 0.018% at 2.8 keV, and 0.026% at 2.98 keV (see Figure 14). The amplitude of the uncertainty on calibration (second term of Equation (41)) is 0.026%, which is an upper limit to the values found at intermediate energies (this upper limit was derived in the worst-case assumption of perfectly correlated contributions in the same spatial and spectral bins).

The fact that the modulation values at 2.7 keV and 2.98 keV coincide with the calibration uncertainty (values written above) proves that the second term of Equation (41) is correct in estimating the uncertainty at the calibration energies.

The discrepancy at the other energies is due to the fact that spurious modulation is linearly interpolated between the values measured at the energies of calibration (2.7 and 2.98 keV), and loses the assumed perfect correlation of the spatial and energy



**Figure 13.** Distribution at 2.7 keV of the centers of observations (each consisting of  $10^4$  iterations, each of which comprises  $10^7$  events) corrected with  $10^3$  different calibration measurements. The difference versus the distribution of Figure 12 is that this is a distribution of the centers of  $10^3$  distributions such as that of Figure 12. The distribution is correctly centered on the true value, with a width given by the calibration uncertainty (second term of Equation (41)).



**Figure 14.** Centers and widths of Stokes parameter  $q$  (the  $u$  case is very similar) obtained from fitting the distributions of calibrations, such as the one in Figure 13, at different energies. The orange lines are the widths computed with Equation (42), centered on the true value (dashed line). The reason for the decrease in width is that the values in between calibration energies are linearly interpolated, and the weighted combination of Equation (42) is more likely to be close to the center if far away from the calibration energies.

bins in Equation (41). The statistical uncertainty on the interpolated value can be obtained with a weighted combination of the values measured at the boundaries:

$$\sigma(E) = \sqrt{\left(\frac{2.98\text{keV} - E}{2.98\text{keV} - 2.7\text{keV}} \sigma_{\text{cal}}^{2.7\text{keV}}\right)^2 + \left(\frac{2.7\text{keV} - E}{2.98\text{keV} - 2.7\text{keV}} \sigma_{\text{cal}}^{2.98\text{keV}}\right)^2}. \quad (42)$$

This expression correctly reproduces the observed values (see Figure 14).

## 6. Conclusion

In this paper, we presented the procedure to calibrate and correct the response to unpolarized radiation of the GPD. First, the method to measure the response of the detector to unpolarized radiation, using two measurements of the same source rotated orthogonally, was presented. Then we discussed a correction algorithm that corrects the systematics for each single event; this allows great flexibility in the subsequent analysis.

The correction done with the photon-by-photon algorithm for monochromatic sources was compared to that obtained as a byproduct of the unpolarized response measurement; the two were shown to provide statistically compatible results. The photon-by-photon algorithm was then analyzed further using calibration data and simulations, proving its spectral capabilities and showing how the correction removes the trend of the systematic effect with energy. This demonstrates that the algorithm is able to subtract the systematic effect, achieving all the sensitivity possible with the GPD.










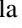

The Italian contribution to the IXPE mission is supported by the Italian Space Agency (ASI) through the contract ASI-OHBI-2017-12-I.0, the agreements ASI-INAF-2017-12-H0 and ASI-INFN-2017.13-H0, and its Space Science Data Center




(SSDC), and by the Istituto Nazionale di Astrofisica (INAF) and the Istituto Nazionale di Fisica Nucleare (INFN) in Italy.

The United States contribution to the IXPE mission is supported by NASA as part of the Small Explorers Program.

*Facility:* Imaging X-ray Polarimetry Explorer (IXPE).

### ORCID iDs

John Rankin  <https://orcid.org/0000-0002-9774-0560>  
 Fabio Muleri  <https://orcid.org/0000-0003-3331-3794>  
 Matteo Bachetti  <https://orcid.org/0000-0002-4576-9337>  
 Enrico Costa  <https://orcid.org/0000-0003-4925-8523>  
 Alessandro Di Marco  <https://orcid.org/0000-0003-0331-3259>  
 Sergio Fabiani  <https://orcid.org/0000-0003-1533-0283>  
 Fabio La Monaca  <https://orcid.org/0000-0001-8916-4156>  
 Paolo Soffitta  <https://orcid.org/0000-0002-7781-4104>  
 Luca Baldini  <https://orcid.org/0000-0002-9785-7726>  
 Niccolò Di Lalla  <https://orcid.org/0000-0002-7574-1298>  
 Alberto Manfreda  <https://orcid.org/0000-0002-0998-4953>  
 Matteo Perri  <https://orcid.org/0000-0003-3613-4409>

Simonetta Puccetti  <https://orcid.org/0000-0002-2734-7835>  
 Carmelo Sgrò  <https://orcid.org/0000-0001-5676-6214>  
 Martin C. Weisskopf  <https://orcid.org/0000-0002-5270-4240>

### References

- Baldini, L., Barbanera, M., Bellazzini, R., et al. 2021, *APh*, 133, 102628  
 Bellazzini, R., Spandre, G., Minuti, M., et al. 2006, *NIMPA*, 566, 552  
 Bellazzini, R., Spandre, G., Minuti, M., et al. 2007, *NIMPA*, 579, 853  
 Costa, E., Soffitta, P., Bellazzini, R., et al. 2001, *Natur*, 411, 662  
 Fabiani, S., Muleri, F., Marco, A. D., et al. 2021, *Proc. SPIE*, 11444, 1029  
 Feng, H., Jiang, W., Minuti, M., et al. 2019, *ExA*, 47, 225  
 Feng, H., Li, H., Long, X., et al. 2020, *NatAs*, 4, 511  
 Kislak, F., Clark, B., Beilicke, M., & Krawczynski, H. 2015, *Aph*, 68, 45  
 Muleri, F., Piazzolla, R., Di Marco, A., et al. 2022, *Aph*, 136, 102658  
 Soffitta, P., Baldini, L., Bellazzini, R., et al. 2021, *AJ*, 162, 208  
 Weisskopf, M. C., Ramsey, B., O'Dell, S., et al. 2016, *Proc. SPIE*, 9905, 990517,  
 Weisskopf, M. C., Silver, E. H., Kestenbaum, H. L., Long, K. S., & Novick, R. 1978, *ApJ*, 220, L117  
 Zhang, S., Santangelo, A., Feroci, M., et al. 2019, *SCPMA*, 62, 29502